Deformation and fracture of 3D printed disordered lattice materials
Experiments and modeling

Xu, Yading; Zhang, Hongzhi; Šavija, Branko; Chaves Figueiredo, Stefan; Schlangen, Erik

DOI
10.1016/j.matdes.2018.11.047

Publication date
2019

Document Version
Final published version

Published in
Materials and Design

Citation (APA)
Xu, Y., Zhang, H., Šavija, B., Chaves Figueiredo, S., & Schlangen, E. (2019). Deformation and fracture of 3D printed disordered lattice materials: Experiments and modeling. *Materials and Design*, *162*, 143-153. https://doi.org/10.1016/j.matdes.2018.11.047

Materials and Design 162 (2019) 143–153

Contents lists available at ScienceDirect

Materials and Design

journal homepage: www.elsevier.com/locate/matdes

Deformation and fracture of 3D printed disordered lattice materials: Experiments and modeling

Yading Xu, Hongzhi Zhang *, Branko Šavija, Stefan Chaves Figueiredo, Erik Schlangen

Microlab, Faculty of Civil Engineering and Geosciences, Delft University of Technology, 2628, CN, Delft, the Netherlands

HIGHLIGHTS

- Three-dimensional disordered lattice materials have been designed and printed using fused deposition modeling.
- Fracture performance of the printed lattice material is simulated by an experiment informed discrete model.
- The influence of printing directions on the lattice material can be captured by the discrete lattice model.
- The influence of disorder degree on the printed materials is experimentally and numerically clarified.

GRAPHICAL ABSTRACT

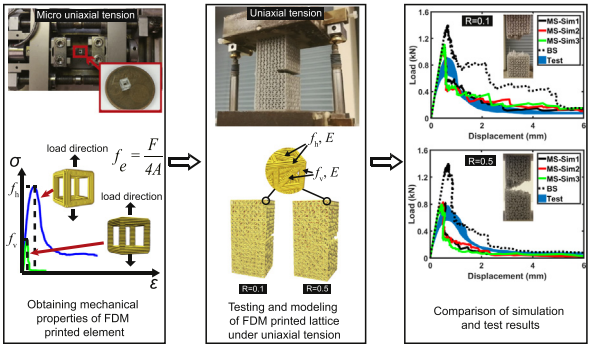

ARTICLE INFO

Article history:
Received 12 October 2018
Received in revised form 21 November 2018
Accepted 22 November 2018
Available online 23 November 2018

Keywords:
Lattice material
Lattice model
Fracture
3D printing
Uniaxial tensile test

ABSTRACT

A method is presented to model deformation and fracture behavior of 3D printed disordered lattice materials under uniaxial tensile load. A lattice model was used to predict crack pattern and load-displacement response of the printed lattice materials. To include the influence of typical layered structures of 3D printed materials in the simulation, two types of printed elements were considered: horizontally and vertically printed elements. Strengths of these elements were measured: 3 mm cubic units consist of lattice elements with two printing directions were printed and their strengths were tested in uniaxial tension. Afterwards, the measured element strengths and bulk material strength, respectively, were used as model input. Uniaxial tensile tests were also performed on the printed lattice materials to obtain their crack pattern and load-displacement curves. Simulations and experimental results were comparatively analyzed. For both levels of disorder considered, only when measured strengths were assigned to the elements with identical printing direction, are the predicted crack patterns and load-displacement curves in agreement with experimental results. The results emphasize the importance of considering printing direction when simulating mechanical performance of 3D printed structures. The influence of disorder on lattice material mechanical properties was discussed based on the experiments and simulations.

1. Introduction

The concept of regular lattice structure is defined as a cellular, reticulated framework or system made up of a large number of uniform elements [1]. Mechanical behavior of materials with regular lattice systems has been intensively studied for several decades because of its lightweight nature and excellent performance [1], such as high specific stiffness [2–5] and high specific strength [2,4,6]. However, more generally, lattice systems with defects, imperfections or non-uniformities are abundant in nature [7,8] and artificial materials [9]. The disorder in lattice systems crucially influences their mechanical performance, for

* Corresponding author.
E-mail address: h.zhang-5@tudelft.nl (H. Zhang).

https://doi.org/10.1016/j.matdes.2018.11.047

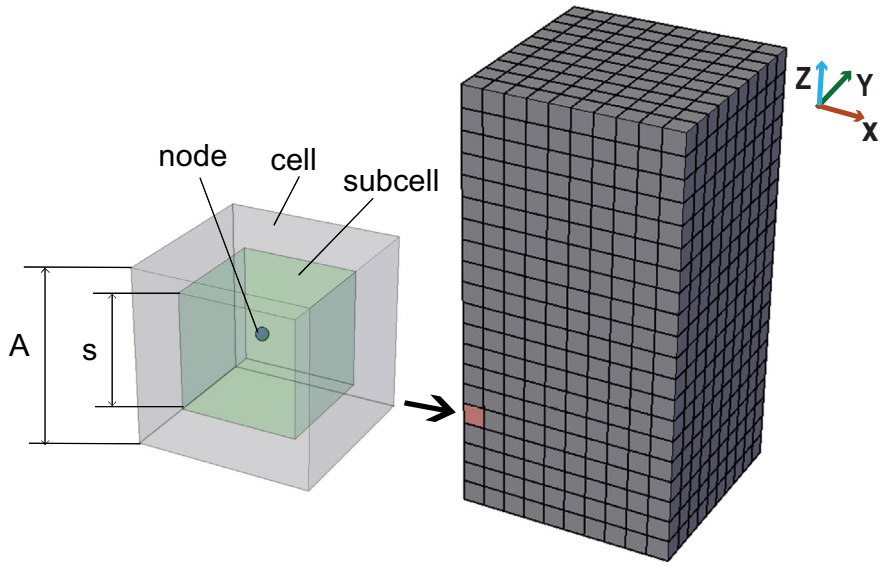

Fig. 1. Discretization of the prismatic domain.

example their elastic and fracture properties [10,11]. Many studies show that the elasticity [12,13] and strength [14,15] of 2D disordered lattice materials are highly dependent on the degree of disorder. Several studies on 3D disordered lattice materials indicate that disorders introduce extra anisotropy to the elastic properties of lattice systems [16,17]. However, fracture behavior and the influence of fabricating process on these 3D disordered lattice materials have not been sufficiently studied.

Owing to the rapid development of additive manufacturing (AM) technology in the past decade, 3D printing methods are becoming widely used for fabricating lattice materials with complex geometries [6,18–20]. A common process for most of 3D printing technique such as fused deposition modeling (FDM) [21,22], selective laser sintering (SLS) [9] and stereolithography (SLA) [23–25], is that materials are precisely deposited layer by layer to build up objects under the control of an automated system to ensure high printing quality even with complex geometries. In general, these layer-wise processing methods introduce anisotropy in printed solid materials, especially in material strength [26–28]. Moreover, there are additional difficulties in studying the mechanical behavior of lattice materials produced by 3D printing, as the lattice structure configuration introduces extra anisotropy [17,29], and each element in the lattice system may have a different printing direction. This may result in considerable variation of lattice element mechanical properties [30–32] and thus may influence the global mechanical behavior of the material. In this case, a proper tool has to be adopted to study mechanical behavior of 3D printed lattice materials, especially their fracture behaviors.

Numerical simulation of mechanical behavior of non-uniform lattice materials has been quite popular in the past decade because complex geometries and disorders can be implemented easily in numerical models [21,33–35]. Among these numerical models, the lattice model is an optimal tool for studying 3D printed lattice materials. The lattice model was first used to study elasticity problem of a continua by Hrennikoff [36] in 1940s. Afterwards the lattice model was adopted in various materials, such as concrete [37], cement paste [38] and nuclear graphite [39]. Commonly the lattice model is used for fracture simulation of continuous materials, but it is still rather suitable for printed lattice materials. On one hand, the lattice system in the model consists of a network of elements which gives the model a geometry that corresponds to lattice materials. This makes it possible to provide detailed deformation and cracking information [40–42] for each single lattice element even in complex lattice geometries. On the other hand, the variation of element properties induced by FDM printing process can also be taken into consideration in the simulation by varying the input properties of each lattice element [40,43,44].

As the lattice model actually uses local element properties to calculate global behavior of the lattice structures [40], correct global structural behavior will be obtained only when correct local element input properties are adopted. To provide reliable simulation results for 3D printed lattice materials, one of the most important questions is proper determination of input mechanical properties for the lattice model [45]. A simple approach is to directly adopt measured properties from bulk materials which is commonly used in the lattice model when simulating quasi-brittle fracture [37,46]. For homogeneous materials, this is a reasonable approximation which results in reliable simulation results. For heterogeneous materials, the size effect [47–49], which may result in considerable differences between local and global mechanical properties, is not considered. In addition, as mentioned before, the anisotropy of printed local lattice elements needs to be taken into account. Therefore, for modeling of 3D printed lattice materials it is necessary to use experimentally measured local element properties as model input to include the influence of printing direction on element mechanical properties.

The main goal of this work is to provide a method for modeling uniaxial tensile response of 3D printed lattice materials. In the presented study, FDM was used to print disordered lattice materials and their lattice beam elements. The mechanical properties of printed lattice elements with different printing directions were tested and used as simulation inputs. The deformation and fracture process of the disordered lattice material were simulated using the Delft lattice model [37,41] to predict its deformation and fracture behavior under uniaxial tension. Afterwards, uniaxial tensile tests were performed on the printed disordered lattice materials. Experiments and simulations are

Table 1
Parameters of generated lattice systems.

No.	Randomness (R)	Cells dimension	Printed lattice material size (mm)	Number of lattice elements	Element radius
L1	0.1	$10 \times 10 \times 20$	$27 \times 27 \times 57$	13,103	0.375
L5	0.5	$10 \times 10 \times 20$	$27 \times 27 \times 57$	12,895	0.375

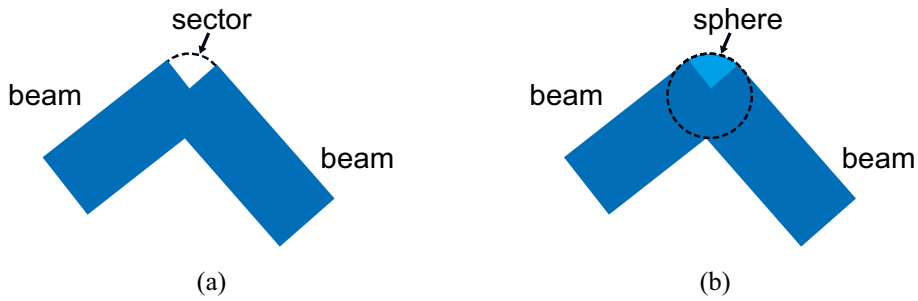

Fig. 2. Connected beams with (a) a sector and (b) a generated sphere.

comparatively analyzed, influence of printing directions and disorder were discussed.

2. Experiments and simulations

2.1. Lattice generation

A method similar to that described in Ref. [50] was used to discretize a domain and generate the lattice network: Two prismatic domains with dimension of 10 cells in length and width, 20 cells in height were generated (Fig. 1). The length of each cell was set to be $A = 3$ mm. Nodes were randomly placed in sub-cells within these cells. In this study, randomness (R) is defined as:

$$R = s/A \tag{1}$$

where s is the length of the sub-cell and A is the length of the cell. The disorder in the lattice material was introduced by including pseudo random numbers generated by random seeds when calculating nodes coordinates. The coordinates of a node in a certain cell which locates in the l-th row in x axis, m-th row in y axis and n-th row in z axis were calculated by the following formulas:

$$\begin{aligned} x_l &= A * ((1-R)/2 + R * r + l - 1) \\ y_m &= A * ((1-R)/2 + R * r + m - 1) \\ z_n &= A * ((1-R)/2 + R * r + n - 1) \end{aligned} \tag{2}$$

where A is the cell length, R is the randomness of the lattice system, r is a random number (generated using a quasi-random number generator in the software with values ranging from 0 to 1) which differs for each node placement, l (integers from 1 to 10) is the cell row number in x axis, m (integers from 1 to 10) is the cell row number in y axis, n (integers from 1 to 20) is the cell row number in z axis. $R = 0$ represents a regular lattice system and $R = 1$ represents a completely disordered lattice system. In this study, two different values of the randomness parameter were considered to generate two lattice systems: 0.1 (s = 0.3 mm) and 0.5 (s = 1.5 mm), respectively.

Node connectivity was determined by Delaunay tessellation and nodes were connected by circular beam elements with a radius of 0.375 mm, forming irregular lattice systems. During the tessellation process, tetrahedrons were generated by connecting nodes making sure no other nodes locate inside the circumsphere of each tetrahedron. The nodes in the surface cells are aligned in a same plane to maintain the prismatic shape of the lattice networks. In the middle of the height direction, a notch is generated in each lattice by removing elements connecting nodes in the outermost two layers from the surface. Parameters of the two irregular lattice systems are shown in Table 1.

Table 2
Configurations of printing parameters.

Printing parameters	Configurations
Layer height (mm)	0.15
Temperature (°C)	195
Filament diameter (mm)	2.85
Nozzle diameter (mm)	0.25
Printing speed (mm/s)	30
Travel speed (mm/s)	120

2.2. Fabrication of lattice materials

In order to ensure the consistency between the printed lattice materials and the lattice systems in the model, the lattice systems generated in Section 2.1 were directly transformed to entities in AutoCAD and printed with polylactic acid (PLA) material using a commercial 3D printer Ultimaker 2+ which is based on FDM. Notice that the lattice elements in the model are only conceptually connected at the nodes, while for entities conceptual elements became actual cylindrical beams with a certain cross section area. When cylindrical beams connect, a sector forms in between (see Fig. 2a). To avoid potential stress concentration near the sector, a sphere with the same radius of the beam was generated at the node in the printed lattice materials (see Fig. 2b).

Considering the principle of FDM, the lattice materials were printed such that the notch was positioned towards the top when printing to ensure good printing quality. Multiple lattice material samples were printed for each randomness. Printing parameters such as layer height, temperature and speed were kept constant for each print and are listed in Table 2. Entity models and printed lattice material samples are shown in Fig. 3.

2.3. Determination of lattice element properties

It should be noted that elements in the printed lattices have different printing directions, and horizontally printed and vertically printed (Fig. 4) elements may have different strength. As a simplification, in this study only two printing directions were assumed: if two nodes of an element located in cells were in one plane parallel to the printing building plane (Fig. 1 plane ZOY), the element was horizontally printed otherwise the element was vertically printed. So, cubic units (Fig. 5) with the same length of the cells (3 mm) were printed. These cubic units were designed to determine the mechanical properties of lattice beams in the two perpendicular printing directions: 4 horizontal beams and 4 vertical beams.

To obtain properties of lattice elements to be used as the input of the lattice model, printed cubic units were glued on small steel blocks (see Fig. 6) using a mix of PLEX 7742 F and Pleximon. Uniaxial tensile tests were performed with an elongating speed of 0.005 mm/s by a Micro Tension-Compression Testing device. For each printing direction, 10 tests were performed.

The strength of one beam in each cubic unit, i.e. the element strength was calculated from measurements by Eq. (3).

$$f_e = \frac{F}{4A} \tag{3}$$

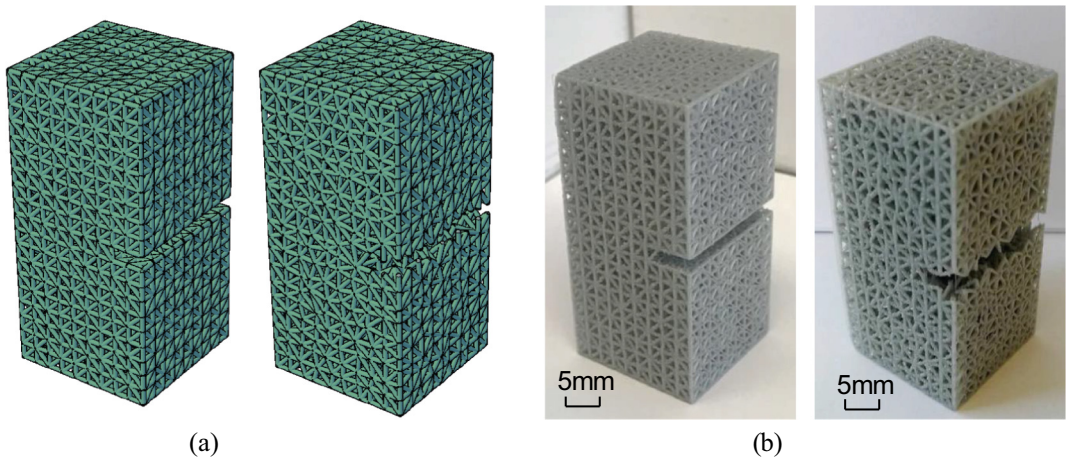

Fig. 3. Comparison of (a) lattice systems with different randomness and (b) corresponding printed lattice materials.

where F is the measured peak load, A is the cross section of a printed small beam. Calculated element strength values of two printing directions are listed in Table 3.

From Table 3 and the load-displacement curves of the horizontally (Fig. 7a) and vertically (Fig. 7b) printed beams in the cubic units, a large difference in strength can be seen between beams in two printing directions. Vertically printed beams are much weaker than horizontally printed beams. Besides, although all beams exhibit softening behaviors after peak load, vertically printed beams are more brittle than horizontally printed beams as vertically printed beams contain layers and interfaces perpendicular to normal stress direction. Fig. 8 shows the calculated work of fracture in post peak branch of two printing directions. Vertically printed beams need much less work to break than horizontally printed beams which is an additional confirmation of higher brittleness of vertically printed beams.

Fractography of fractured beams in two printing directions were obtained by scanning electron microscope (SEM). Samples were coated with carbon to provide conductivity and avoid electrons accumulating on the surface. Subsequently, secondary electrons (SE) were used to obtain the images from the fractured surface of horizontally and vertically printed beams, as shown in Fig. 9. A layered structure consisting of individual filaments resulted from horizontal printing process can be observed on horizontally printed beam in Fig. 9a. Typical necking initiated fracture in polymers [31,51], delaminated single filament and craze of ductile facture [52] are also obvious. For a vertically printed beam, traces of brittle fracture can be found. A rough fracture surface is quite clear in Fig. 9b, which is an evidence of fast fracture under normal stress [30]. The difference in the two fracture surfaces also indicates that beams printed in the two directions exhibit different mechanical properties under tensile load: horizontally printed beams are stronger and more ductile than vertically printed beams.

2.4. Uniaxial tensile tests on printed lattice materials

The printed lattice materials were glued using a mix of PLEX 7742F and Pleximon on two parallel steel plates. Two linear variable differential transformers (LVDTs) were fixed along both lateral sides for measuring displacement (Fig. 10). A displacement controlled uniaxial tensile test with an elongating speed of 0.003 mm/s were conducted on the printed lattice materials by a servo hydraulic press (Instron 8872). For each test, a load-displacement curve was obtained.

2.5. Lattice fracture modeling

In order to simplify the simulation, elastic brittle properties were assumed for the elements in the lattice model (the influence of this assumption on simulation results is discussed in detail in Section 3). Considering the small size of printed cube units, it was not possible to accurately measure the displacement using an LVDT. As a result, the measured displacement was much higher than real values because the recorded data contained a considerable amount of displacement from the loading and transmission

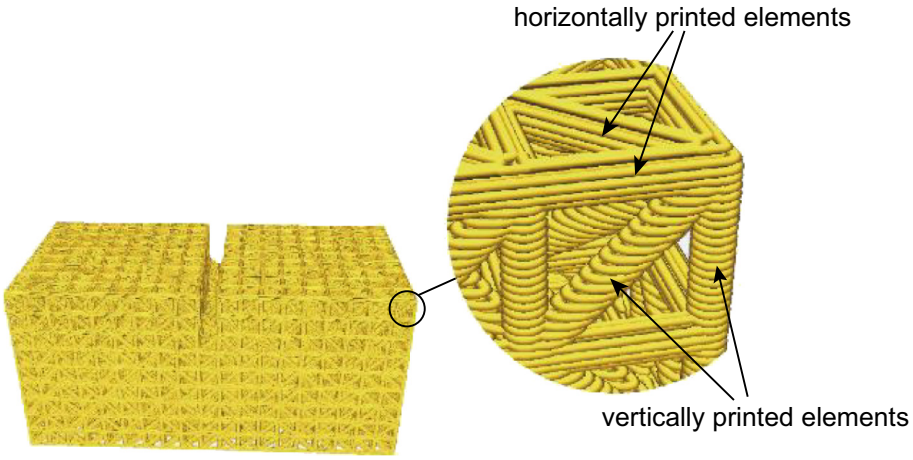

Fig. 4. Elements of two printing directions, showing layers resulting from the FDM printing process.

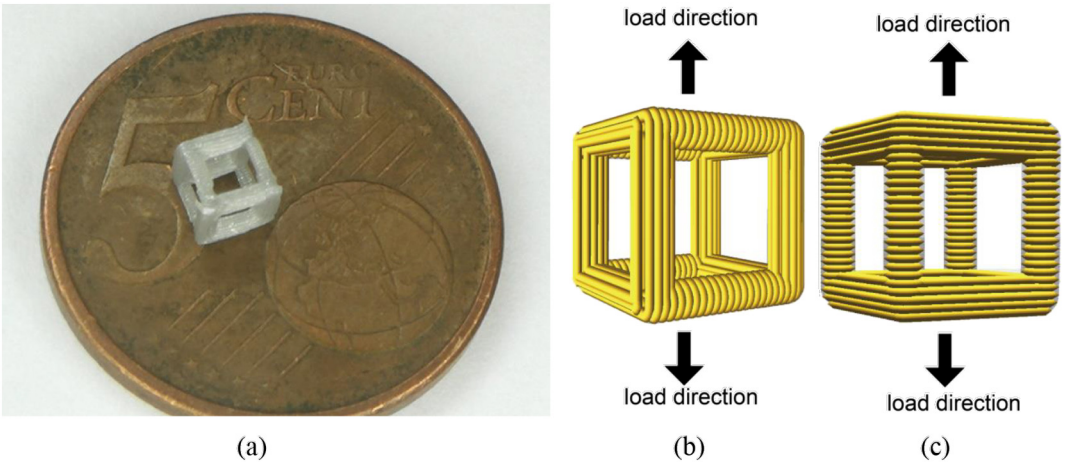

Fig. 5. Printed cubic unit (a) and scheme of loading directions on unit cube for element property determination of (b) horizontally printed elements and (c) vertically printed elements.

mechanisms not only from the tested specimen. Therefore, only measured strength values were adopted directly as the model inputs. Elastic modulus was directly adopted from the material properties provided by the manufacturer for all elements (E = 2346.5 MPa) and Poisson's ratio: $\nu = 0.36$ was adopted as reported in [53,54]. Shear modulus G was calculated by Eq. (4). Note that, in general, Eq. (4) is valid for isotropic materials. According to previous studies [28,30,32,55–58], anisotropy should be considered when exceeding elastic region (e.g. strength), while printing direction has limited influence on the isotropy of elastic properties (both shear and tensile) of printed polymer solid objects. So, shear modulus of printed PLA can be still regarded as isotropic thus Eq. (4) was considered valid and was used to calculate the shear modulus of the printed elements.

$$G = \frac{E}{2(1+\nu)} \tag{4}$$

For both printing directions, pseudo random numbers were used to assign the experimentally determined strength values (see Table 3) to elements with the same printing direction and simulation was executed three times for each lattice system (L1 and L5).

The computing process and post processing methods were similar as reported in [40]. A set of linear elastic analyses was performed under a uniform prescribed displacement boundary condition imposed on top of the lattice system while the bottom elements were clamped. Elements on the top and bottom layers were prohibited from failure in order to maintain the path of force transferring. Comparative stress of beam elements was calculated in each step according to Eq. (5).

$$\sigma = \alpha_N \frac{N}{A} + \alpha_M \frac{\max(|M_i|, |M_j|)}{W} \tag{5}$$

where N is the normal force in the lattice element, A is the cross section of the lattice element, M_i and M_j are the bending moments in the nodes i and j. W is the section modulus, α_N is normal force influencing factor, α_M is bending influence factor. Herein, the influencing factors are taken as $\alpha_N = 1$ and $\alpha_M = 0.05$.

Loading is increased until exactly one beam in the mesh has a stress/strength ratio equal to one in every step until the entire lattice system failed. After the simulation finished, crack pattern was visualized based on the removed elements and load-displacement curve was extracted. Results are shown and analyzed in Section 3.

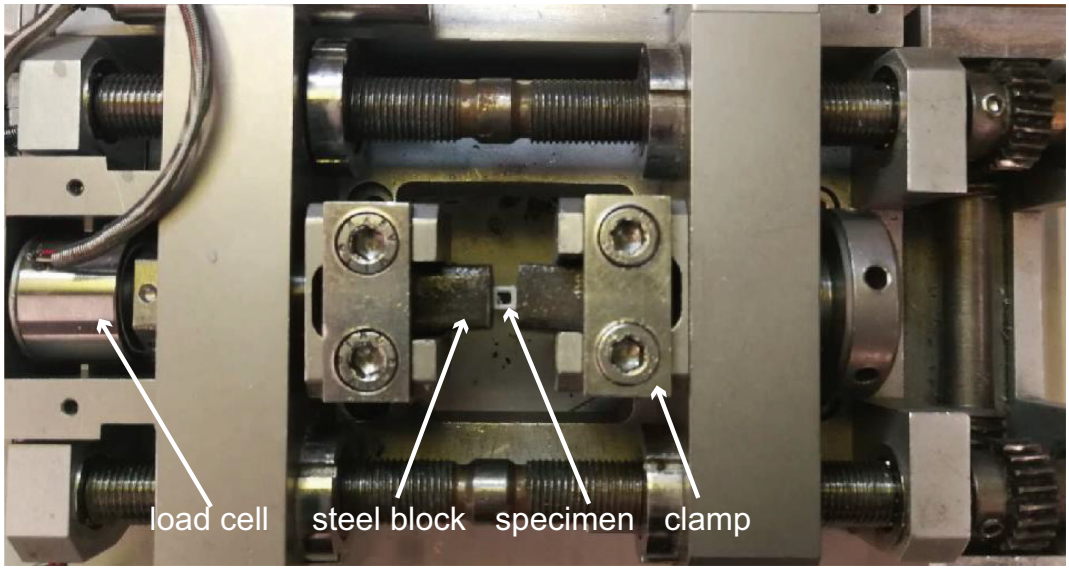

Fig. 6. Experiment setup used for element strength determination.

Table 3
Calculated element strength values of two printing directions (MPa).

Printing direction	Test 1	Test 2	Test 3	Test 4	Test 5	Test 6	Test 7	Test 8	Test 9	Test 10	Average	Standard deviation
Horizontal	35.42	40.71	36.19	38.44	33.04	34.53	42.09	40.08	43.52	33.98	37.80	3.67
Vertical	16.45	13.00	14.20	13.28	8.40	12.51	11.86	13.25	11.29	8.50	12.27	2.45

3. Results and discussion

3.1. Load-displacement response

As a comparison for load-displacement response simulation, bulk material properties (f_e = 49.5 MPa and E = 2346.5 MPa) provided by the manufacturer were also used in a simulation as a baseline case. This was compared to the simulations which use experimental data as input, as previously described. As can be seen in Fig. 11, for (a) L1 and (b) L5, the influence of element strengths is rather obvious. When measured strengths were assigned to corresponding elements in the model, the predicted load-displacement curves (MS-Sim 1, MS-Sim 2 and MS-Sim 3) including stiffness, strength, ductile part and long softening tails are in good accordance with test results (blue shadowed area).

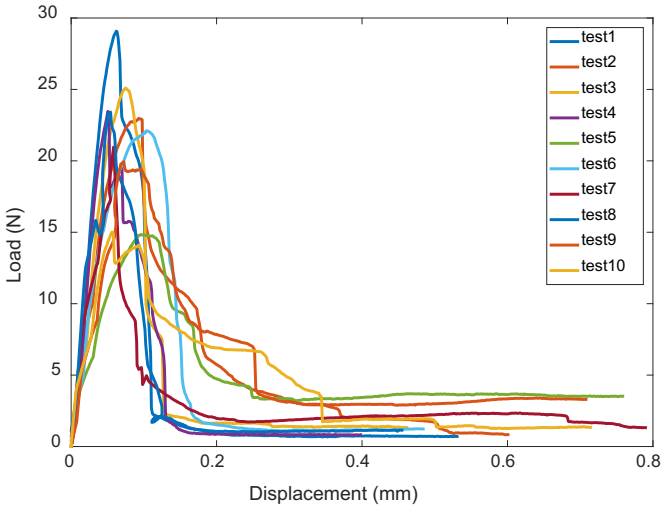

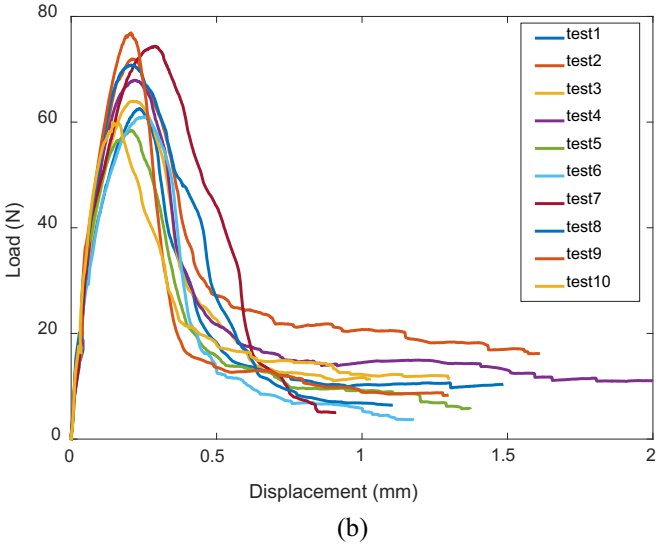

Fig. 7. Load-displacement curves of (a) vertically printed and (b) horizontally printed elements. Note that the axes in the graphs are different and vertically printed elements are much weaker than horizontally printed elements.

Comparatively, the simulated curve using bulk material strength (BS) deviates significantly from the test results. As the bulk materials strength is higher than the strengths of printed lattice elements (especially the strength of vertically printed elements), the simulated peak-load values are much higher for both lattice materials. This means that the element strength is a crucial influence factor in the simulation and only when the input strength is properly assigned are the simulation result accurate.

Normally, the anisotropy of 3D printed solid material mainly lies in strength and it is dominated by printing direction [26–28]. In lattice materials, however, and additional feature is present. The lattice structure itself introduces additional anisotropy to the material. The influence of printing direction is coupled with the influence of lattice element orientation. Because both vertically and horizontally printed lattice elements are present in the lattice material simultaneously and their strengths are different (Table 3), using constant bulk material properties (i.e. strength of PLA as provided by the manufacturer) as simulation input will not result in a correct output of the simulation. In this case, measured properties (PLA "strengths" on mesoscale in two printing directions) of local lattice elements in different printing directions are necessary. The comparison of simulation results using constant bulk property (PLA strength on macroscale) and measured local element properties (PLA "strengths" on mesoscale) gives insight of the influence of the printing process on the anisotropy of 3D printed lattice materials. Furthermore, it emphasizes that the anisotropy of 3D printed lattice materials comes from both the printing direction and the lattice element orientation.

Still, even measured strengths were correctly assigned as model element inputs, some mismatches in the softening part can be observed from Fig. 11 for both lattice materials. First, the elastic modulus of the material was taken as provided by the manufacturer, which is probably somewhat higher compared to the printed one. This resulted in a somewhat higher stiffness in the simulations compared to the experiments. Note, also, that in the simulation lattice beam elements are all considered to be perfectly brittle. In reality, the elements in the printed lattice materials exhibited softening after peak load, dependent on the printing direction (see Fig. 7). It is clear that the printed lattice materials have a less-brittle softening branch than predicted due to the fact that, in the simulation, softening on the element level was not considered. Note

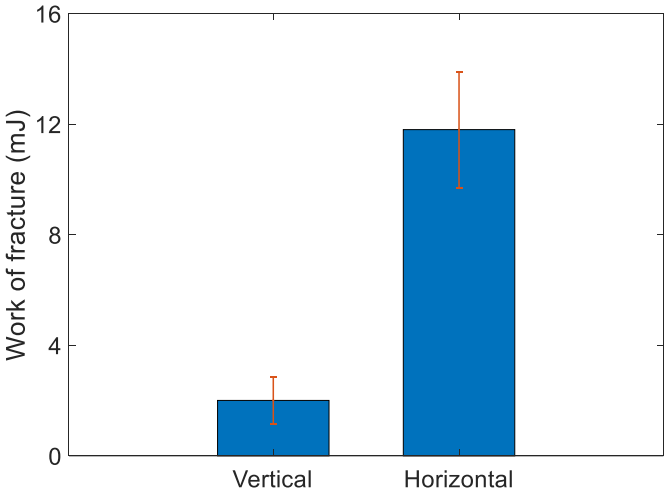

Fig. 8. Work of fracture of elements in two printing directions (standard deviation is indicated).

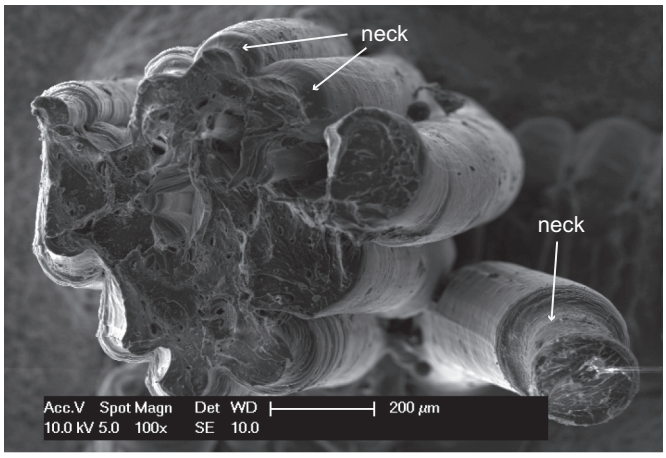

(a)

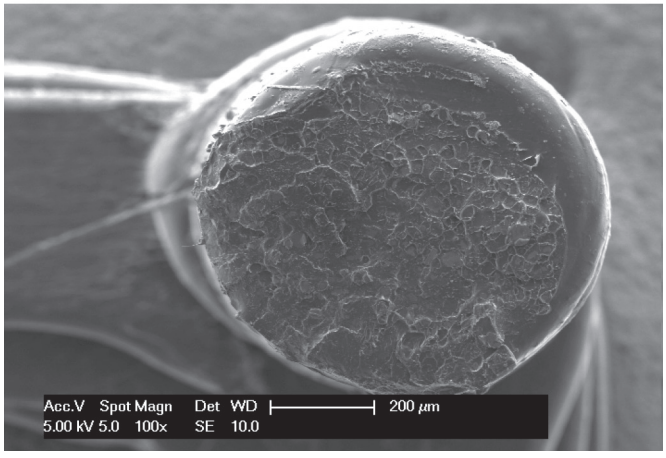

(b)

Fig. 9. Fracture surface of (a) horizontally printed beam and (b) vertically printed beam.

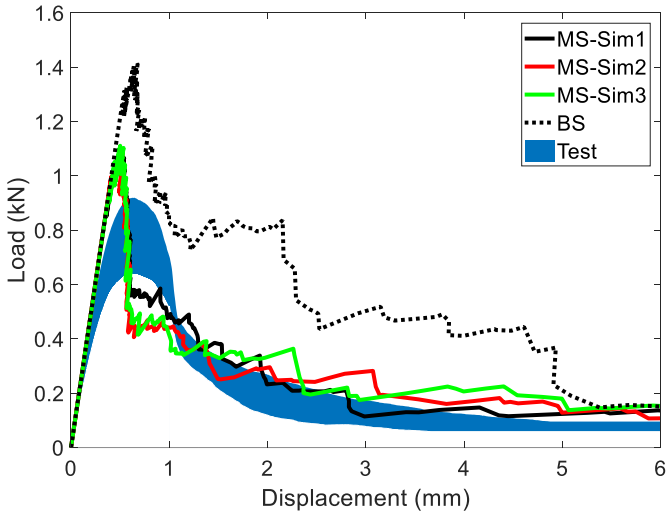

(a)

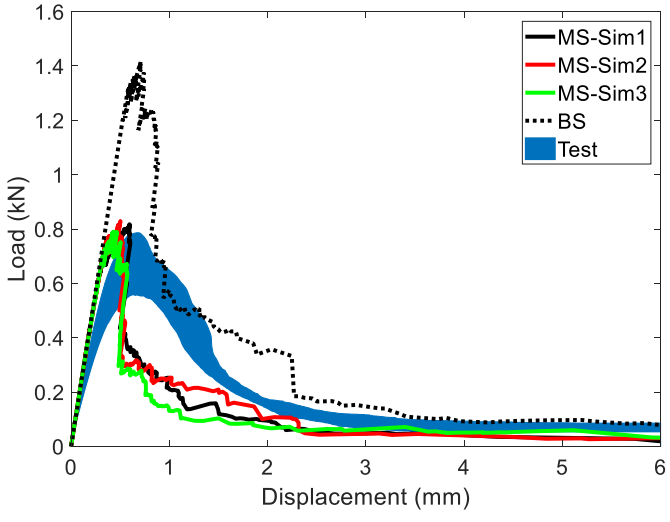

(b)

Fig. 11. Simulated Load-displacement curves of (a) L1 and (b) L5 against experiment results.

that, in the model, ductility or softening behavior can be introduced by assigning multi-linear properties (e.g. shown in Fig. 12) to the elements [59,60]. In this case, the element loses its strength and stiffness

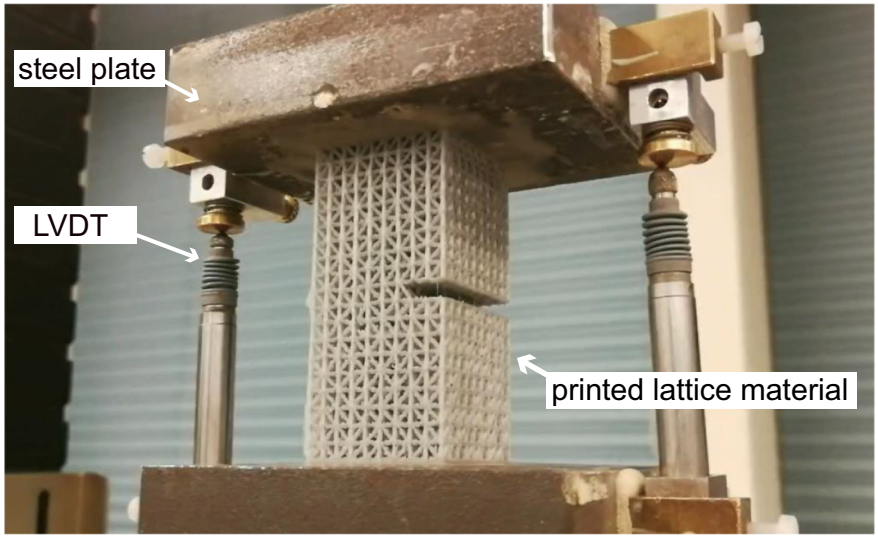

Fig. 10. Uniaxial tensile test setup for printed lattice materials.

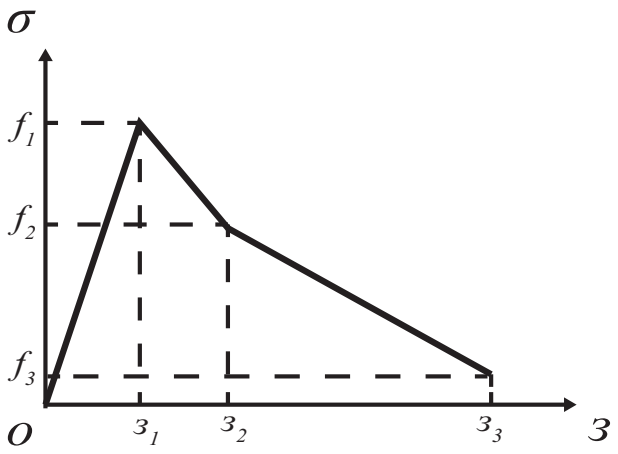

Fig. 12. Multilinear properties of lattice element.

gradually and is eventually removed from the lattice system through several analysis steps. Since the data relating to these properties could not be measured reliably in this study (see Section 2.3), this was not done herein.

The difference between virtual lattice systems and actual lattice materials also resulted in some mismatches in terms of strength. As described in Section 2.2, in the lattice model nodes only conceptually exist and never fail, while in printed lattice materials nodes were actually generated as spheres and fractures at the spheres can be found in experiment. When spheres failed first and connected elements were unable to fail, the required external load to break the spheres was lower than breaking the connected beams and the peak load (Table 4) obtained from the experiment were lower than simulated value as a result. However, in the lattice model, this mechanism is not considered.

The influence of randomness on the load-displacement response of lattice materials was properly predicted by the simulation. Because more artificial disorder was introduced to lattice system with randomness $R = 0.5$ it exhibited lower stiffness and lower peak load than lattice system with $R = 0.1$ and this trend can also be found in the experiment results (Table 4).

3.2. Influence of randomness on crack patterns

Figs. 13 and 14 show the simulated and experimentally obtained crack patterns of two lattice systems and printed lattice materials respectively. The crack patterns predicted by the lattice model are in good accordance with the experiment results. In the simulated results, crack patterns before and after peak load are indicated in different colors. In L1 (R = 0.1), a main crack plane traversed across the lattice system in the middle (Fig. 13). Almost all failed elements localized in the main crack plane before and after peak load, with only a few failed elements distributed out of the main crack plane. In L5 (R = 0.5), on the other hand, numerous failed elements distributed in the non-notched side before peak load which means L5 exhibit more ductility as more artificial disorder was introduced. After peak load, failed elements started to localize in the main crack plane in the middle. There are still many elements distributing out of the main crack plane at the

Table 4
Simulated strength and stiffness results against experiment data.

Group	Randomness	Slope (kN/mm)	Peak load (kN)
Simulation	0.1	2.434 ± 0.007	1.093 ± 0.013
	0.5	2.293 ± 0.000	0.812 ± 0.020
Experiment	0.1	2.055 ± 0.351	0.765 ± 0.143
	0.5	1.568 ± 0.327	0.658 ± 0.112

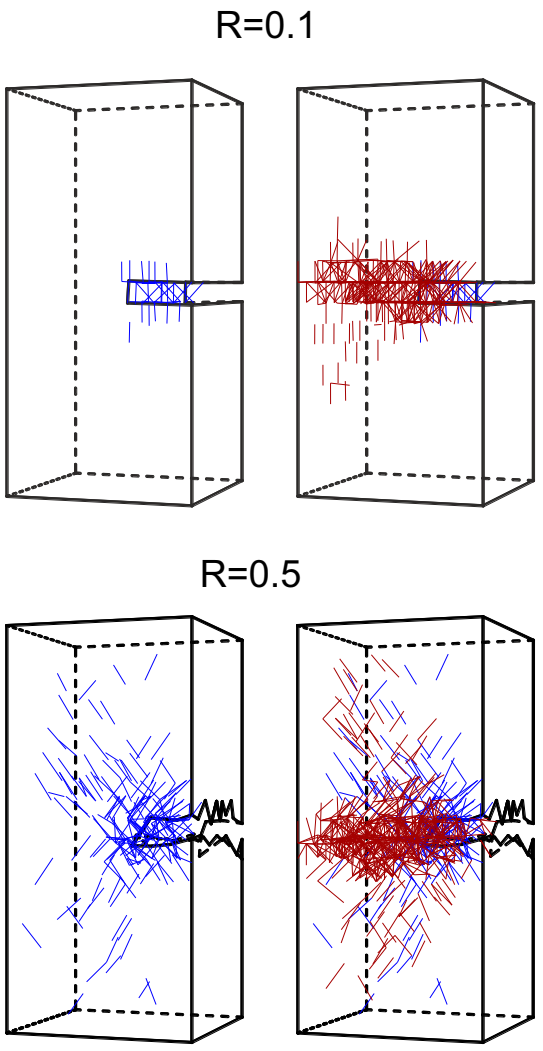

Fig. 13. Simulated crack patterns before peak load (blue elements) and after peak load (red elements). Figures on the left show cracks at maximum load, while on the right they show cracks at failure. (For interpretation of the references to color in this figure legend, the reader is referred to the web version of this article.)

unnotched side and less brittleness of L5 can be expected during softening. Similarly, in the experiment results (see Fig. 14), crack plane is also mainly located within the elements in the middle of the sample in lattice materials with R = 0.1 while concaved and convex crack surface can be observed from fractured lattice materials with $R = 0.5$.

The influence of randomness on the crack pattern can be explained by the fact that the strain non-uniformity appeared in the lattice system as heterogeneities were introduced and stress concentration appeared near the notch when external load was imposed. For L1, elements near the notch and further away from the notch are elastically similar owing to the rather regular nodes distribution. When the external load was applied, stress concentration appeared near the notch and the elements close to the notch had higher stress/strength ratio than other elements so that the crack initiated in these elements and propagated across the lattice material from the notch forming a main crack plane. Because the randomness was 0.1 not 0, some artificial disorder existed, there are still a few failed elements out of the main crack plane. For beam lattice systems, increasing randomness introduces more disorder into the system. Therefore, for L5 elastic modulus differs in regions within the irregular lattice system. Note that the cross section of all beams is equal. In regions with closer node spacing a denser material is created, which results in a higher local elastic modulus. Elements in lower elastic modulus regions were forced to exhibit more strain and

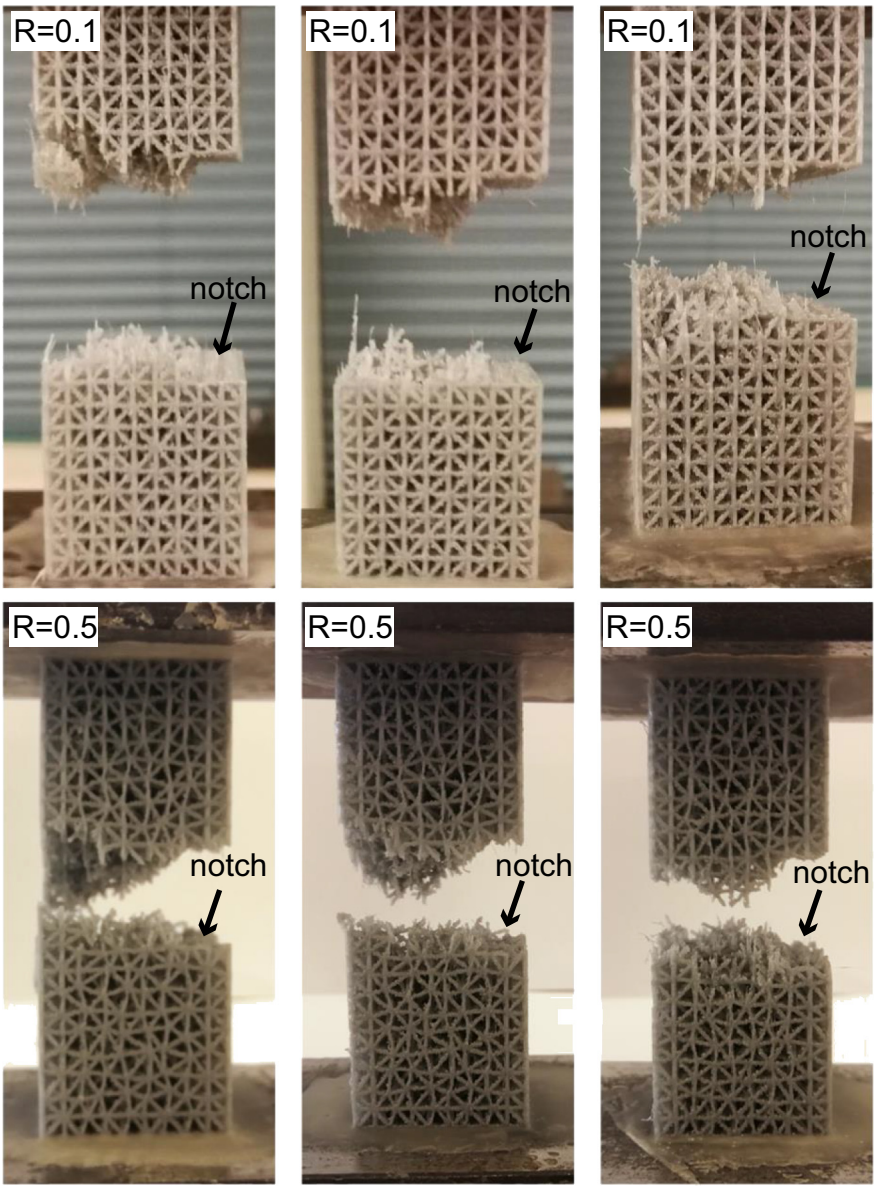

Fig. 14. Fractured lattice materials.

the stress in the elements were higher than other elements which made them easier to fail than other elements. As a result, concaved main crack plane and plenty of failed elements out of the main crack plane can be observed.

4. Conclusions

In this study, lattice materials with different randomness were 3D printed using FDM and a numerical lattice model with the same geometries was used to analyze their deformation and fracture behaviors under uniaxial tensile load. Properties of the lattice elements with different printing directions were experimentally determined. According to the experiment results, element mechanical properties vary with printing directions. During simulation, experimentally measured strengths were assigned to elements with identical printing direction as model input. As a simplification, linear elastic-perfectly brittle properties were assumed and also assigned to the elements in the model. Crack patterns and load-displacement responses of the printed lattice materials were predicted by the simulation. Afterwards, actual uniaxial tensile tests were conducted on the printed lattice materials. By comparing and analyzing simulated and experiment results, some conclusions can be drawn as below:

- According to experiments and simulations, lattice materials with higher randomness exhibit lower stiffness, lower strength and less brittleness since higher randomness introduces more disorder to the lattice system resulting in more scattered distribution of failed elements.
- Anisotropy introduced by both printing directions and structure configuration of such 3D printed lattice materials can be taken into account in the modeling using the approach proposed herein. Using the experimentally determined elements strength as inputs, the lattice model can accurately predict the fracture behavior and load-displacement response of 3D printed lattice materials in uniaxial tensile test. Comparatively, neglecting of the variation of element strength introduced by the printing direction makes it impossible to obtain accurate simulation results.

As a result of the assumed ideally brittle behavior of the lattice elements, a mismatch in the softening part of the post-peak branch between the simulations and the experiments was. In fact, actual lattice

materials exhibit wider softening part than the simulations. Further research will focus on the determination of multi-linear properties for elements to perform more accurate prediction.

CRediT authorship contribution statement

Yading Xu: Methodology, Data curation, Writing - original draft. **Hongzhi Zhang:** Methodology, Writing - review & editing. **Branko Šavija:** Writing - review & editing, Supervision. **Stefan Chaves Figueiredo:** Methodology. **Erik Schlangen:** Funding acquisition, Writing - review & editing, Supervision.

Acknowledgements

Yading Xu and Hongzhi Zhang would like to acknowledge the funding supported by China Scholarship Council (CSC) under the grant CSC No. 201708110187 and No. 201506120067. Stefan Chaves Figueiredo would like to acknowledge the funding from Science Without Borders from the National Council for Scientific and Technological Development (CNPq) of Brazil (201620/2014-6). The authors would like to acknowledge Mr. Maiko van Leeuwen for his support in the mechanical tests and Mr. Arjan Thijssen for his assistance in SEM work.

References

[1] N.A. Fleck, V.S. Deshpande, M.F. Ashby, Micro-architectured materials: past, present and future, Proceedings of the royal society of London a: mathematical, physical and engineering sciences, Vol. 466, 2121, The Royal Society September 2010, pp. 2495–2516.
[2] B.G. Compton, J.A. Lewis, 3D-printing of lightweight cellular composites, Adv. Mater. 26 (34) (2014) 5930–5935.
[3] V.S. Deshpande, N.A. Fleck, M.F. Ashby, Effective properties of the octet-truss lattice material, J. Mech. Phys. Solids 49 (8) (2001) 1747–1769.
[4] L. Dong, V. Deshpande, H. Wadley, Mechanical response of Ti–6Al–4V octet-truss lattice structures, Int. J. Solids Struct. 60 (2015) 107–124.
[5] M.S. Elsayed, D. Pasini, Analysis of the elastostatic specific stiffness of 2D stretching-dominated lattice materials, Mech. Mater. 42 (7) (2010) 709–725.
[6] J. Bauer, S. Hengsbach, I. Tesari, R. Schwaiger, O. Kraft, High-strength cellular ceramic composites with 3D microarchitecture, Proc. Natl. Acad. Sci. 111 (7) (2014) 2453–2458.
[7] L.J. Gibson, Biomechanics of cellular solids, J. Biomech. 38 (3) (2005) 377–399.
[8] T.M. Keaveny, E.F. Morgan, G.L. Niebur, O.C. Yeh, Biomechanics of trabecular bone, Annu. Rev. Biomed. Eng. 3 (1) (2001) 307–333.
[9] N. Takano, H. Takizawa, P. Wen, K. Odaka, S. Matsunaga, S. Abe, Stochastic prediction of apparent compressive stiffness of selective laser sintered lattice structure with geometrical imperfection and uncertainty in material property, Int. J. Mech. Sci. 134 (2017) 347–356.
[10] E. Schlangen, E.J. Garboczi, New method for simulating fracture using an elastically uniform random geometry lattice, Int. J. Eng. Sci. 34 (10) (1996) 1131–1144.
[11] G. Lilliu, J.G.M. Van Mier, M.R.A. van Vliet, Numerical characterization of the elastic properties of heterogeneous materials with a 3D lattice model, WIT Transactions on Modelling and Simulation, 22, , 1999.
[12] S. Liebenstein, S. Sandfeld, M. Zaiser, Size and disorder effects in elasticity of cellular structures: from discrete models to continuum representations, Int. J. Solids Struct. 146 (2018) 97–116.
[13] T. Mukhopadhyay, S. Adhikari, Effective in-plane elastic moduli of quasi-random spatially irregular hexagonal lattices, Int. J. Eng. Sci. 119 (2017) 142–179.
[14] A. Fazekas, R. Dendievel, L. Salvo, Y. Bréchet, Effect of microstructural topology upon the stiffness and strength of 2D cellular structures, Int. J. Mech. Sci. 44 (10) (2002) 2047–2066.
[15] A. Ajdari, H. Nayeb-Hashemi, P. Canavan, G. Warner, Effect of defects on elastic–plastic behavior of cellular materials, Mater. Sci. Eng. A 487 (1–2) (2008) 558–567.
[16] W. Zhu, N. Blal, S. Cunsolo, D. Baillis, Micromechanical modeling of effective elastic properties of open-cell foam, Int. J. Solids Struct. 115 (2017) 61–72.
[17] O.E. Sotomayor, H.V. Tippur, Role of cell regularity and relative density on elastoplastic compression response of 3-D open-cell foam core sandwich structure generated using Voronoi diagrams, Acta Mater. 78 (2014) 301–313.
[18] M.T. Andani, M.R. Karamooz-Ravari, R. Mirzaeifar, J. Ni, Micromechanics modeling of metallic alloys 3D printed by selective laser melting, Mater. Des. 137 (2018) 204–213.
[19] M. Xia, J. Sanjayan, Method of formulating geopolymer for 3D printing for construction applications, Mater. Des. 110 (2016) 382–390.
[20] T. Bückmann, N. Stenger, M. Kadic, J. Kaschke, A. Frölich, T. Kennerknecht, ... M. Wegener, Tailored 3D mechanical metamaterials made by dip-in direct-laser-writing optical lithography, Adv. Mater. 24 (20) (2012) 2710–2714.
[21] M. Kaur, T.G. Yun, S.M. Han, E.L. Thomas, W.S. Kim, 3D printed stretching-dominated micro-trusses, Mater. Des. 134 (2017) 272–280.
[22] M. Kucewicz, P. Baranowski, J. Małachowski, A. Popławski, P. Płatek, Modelling, and characterization of 3D printed cellular structures, Mater. Des. 142 (2018) 177–189.
[23] J. Holländer, R. Hakala, J. Suominen, N. Moritz, J. Yliruusi, N. Sandler, 3D printed UV light cured polydimethylsiloxane devices for drug delivery, Int. J. Pharm. 544 (2) (2018) 433–442.
[24] H. Xing, B. Zou, S. Li, X. Fu, Study on surface quality, precision and mechanical properties of 3D printed ZrO2 ceramic components by laser scanning stereolithography, Ceram. Int. 43 (18) (2017) 16340–16347.
[25] R. He, W. Liu, Z. Wu, D. An, M. Huang, H. Wu, ... Z. Xie, Fabrication of complex-shaped zirconia ceramic parts via a DLP-stereolithography-based 3D printing method, Ceram. Int. 44 (3) (2018) 3412–3416.
[26] A.R. Torrado, D.A. Roberson, Failure analysis and anisotropy evaluation of 3D-printed tensile test specimens of different geometries and print raster patterns, J. Fail. Anal. Prev. 16 (1) (2016) 154–164.
[27] A. Lanzotti, M. Grasso, G. Staiano, M. Martorelli, The impact of process parameters on mechanical properties of parts fabricated in PLA with an open-source 3-D printer, Rapid Prototyp. J. 21 (5) (2015) 604–617.
[28] R. Zou, Y. Xia, S. Liu, P. Hu, W. Hou, Q. Hu, C. Shan, Isotropic and anisotropic elasticity and yielding of 3D printed material, Compos. Part B 99 (2016) 506–513.
[29] S. Xu, J. Shen, S. Zhou, X. Huang, Y.M. Xie, Design of lattice structures with controlled anisotropy, Mater. Des. 93 (2016) 443–447.
[30] Y. Song, Y. Li, W. Song, K. Yee, K.Y. Lee, V.L. Tagarielli, Measurements of the mechanical response of unidirectional 3D-printed PLA, Mater. Des. 123 (2017) 154–164.
[31] A.R.T. Perez, D.A. Roberson, R.B. Wicker, Fracture surface analysis of 3D-printed tensile specimens of novel ABS-based materials, J. Fail. Anal. Prev. 14 (3) (2014) 343–353.
[32] J.M. Chacón, M.A. Caminero, E. García-Plaza, P.J. Núñez, Additive manufacturing of PLA structures using fused deposition modelling: effect of process parameters on mechanical properties and their optimal selection, Mater. Des. 124 (2017) 143–157.
[33] D. Ruffoni, J. William Chapman Dunlop, P. Fratzl, R. Weinkamer, Effect of minimal defects in periodic cellular solids, Philos. Mag. 90 (13) (2010) 1807–1818.
[34] A. Rafsanjani, D. Derome, J. Carmeliet, The role of geometrical disorder on swelling anisotropy of cellular solids, Mech. Mater. 55 (2012) 49–59.
[35] M.H. Luxner, A. Woesz, J. Stampfl, P. Fratzl, H.E. Pettermann, A finite element study on the effects of disorder in cellular structures, Acta Biomater. 5 (1) (2009) 381–390.
[36] A. Hrennikoff, Framework Method and its Technique for Solving Plane Stress Problems, 9, Publ. International Association Bridge Structure Engineering, 1949 217–247.
[37] H.E.J.G. Schlangen, Experimental and Numerical Analysis of Fracture Processes in Concrete, 1993.
[38] H. Zhang, B. Šavija, S.C. Figueiredo, E. Schlangen, Experimentally validated multi-scale modelling scheme of deformation and fracture of cement paste, Cem. Concr. Res. 102 (2017) 175–186.
[39] B. Šavija, D. Liu, G. Smith, K.R. Hallam, E. Schlangen, P.E. Flewitt, Experimentally informed multi-scale modelling of mechanical properties of quasi-brittle nuclear graphite, Eng. Fract. Mech. 153 (2016) 360–377.
[40] Z. Qian, Multiscale Modeling of Fracture Processes in Cementitious Materials, 2012.
[41] E. Schlangen, J.G.M. Van Mier, Simple lattice model for numerical simulation of fracture of concrete materials and structures, Mater. Struct. 25 (9) (1992) 534–542.
[42] M. Nikolić, E. Karavelić, A. Ibrahimbegovic, P. Miščević, Lattice element models and their peculiarities, Arch. Comput. Meth. Eng. 25 (3) (2018) 753–784.
[43] J.G. Van Mier, M.R. van Vliet, T.K. Wang, Fracture mechanisms in particle composites: statistical aspects in lattice type analysis, Mech. Mater. 34 (11) (2002) 705–724.
[44] Z. Qian, G. Ye, E. Schlangen, K. van Breugel, 3D lattice fracture model: application to cement paste at microscale, Key Engineering Materials, Vol. 452, Trans Tech Publications 2011, pp. 65–68.
[45] J.G. Van Mier, Concrete fracture: a multiscale approach, CRC Press, 2012.
[46] R. Ince, A. Arslan, B.L. Karihaloo, Lattice modelling of size effect in concrete strength, Eng. Fract. Mech. 70 (16) (2003) 2307–2320.
[47] Z.P. Bažant, Size effect on structural strength: a review, Arch. Appl. Mech. 69 (9–10) (1999) 703–725.
[48] T.S. Guruprasad, S. Bhattacharya, S. Basu, Size effect in microcompression of polystyrene micropillars, Polymer 98 (2016) 118–128.
[49] J.R. Greer, J.T.M. De Hosson, Plasticity in small-sized metallic systems: intrinsic versus extrinsic size effect, Prog. Mater. Sci. 56 (6) (2011) 654–724.
[50] M. Yip, J. Mohle, J.E. Bolander, Automated modeling of three-dimensional structural components using irregular lattices, Comput. Aided Civ. Inf. Eng. 20 (6) (2005) 393–407.
[51] A.R. Torrado, C.M. Shemelya, J.D. English, Y. Lin, R.B. Wicker, D.A. Roberson, Characterizing the effect of additives to ABS on the mechanical property anisotropy of specimens fabricated by material extrusion 3D printing, Addit. Manuf. 6 (2015) 16–29.
[52] E.S. Greenhalgh, Delamination-dominated Failures in Polymer Composites, CRC Press, 2009.
[53] J. Torres, J. Cotelo, J. Karl, A.P. Gordon, Mechanical property optimization of FDM PLA in shear with multiple objectives, JOM 67 (5) (2015) 1183–1193.
[54] G.W. Melenka, J.S. Schofield, M.R. Dawson, J.P. Carey, Evaluation of dimensional accuracy and material properties of the MakerBot 3D desktop printer, Rapid Prototyp. J. 21 (5) (2015) 618–627.
[55] M. Domingo-Espin, J.M. Puigoriol-Forcada, A.A. Garcia-Granada, J. Lluma, S. Borros, G. Reyes, Mechanical property characterization and simulation of fused deposition modeling polycarbonate parts, Mater. Des. 83 (2015) 670–677.
[56] S. Bhandari, R. Lopez-Anido, Finite element analysis of thermoplastic polymer extrusion 3D printed material for mechanical property prediction, Addit. Manuf. 22 (2018) 187–196.

[57] W.C. Smith, R.W. Dean, Structural characteristics of fused deposition modeling polycarbonate material, Polym. Test. 32 (8) (2013) 1306–1312.
[58] O.S. Es-Said, J. Foyos, R. Noorani, M. Mendelson, R. Marloth, B.A. Pregger, Effect of layer orientation on mechanical properties of rapid prototyped samples, Mater. Manuf. Process. 15 (1) (2000) 107–122.
[59] B.L. Karihaloo, P.F. Shao, Q.Z. Xiao, Lattice modelling of the failure of particle composites, Eng. Fract. Mech. 70 (17) (2003) 2385–2406.
[60] D. Liu, B. Šavija, G.E. Smith, P.E. Flewitt, T. Lowe, E. Schlangen, Towards understanding the influence of porosity on mechanical and fracture behaviour of quasi-brittle materials: experiments and modelling, Int. J. Fract. 205 (1) (2017) 57–72.